nanomaterials

MDPI

Article

The Various Packing Structures of Tb@C_{82} (I, II) Isomers in Their Cocrystals with Ni(OEP)

Wei Dong [1], Qin Zhou [1], Wangqiang Shen [2], Le Yang [3], Peng Jin [3], Xing Lu [2,*] and Yongfu Lian [1,*]

[1] Key Laboratory of Functional Inorganic Material Chemistry, Ministry of Education, School of Chemistry and Materials Science, Heilongjiang University, Harbin 150080, China
[2] State Key Laboratory of Materials Processing and Die & Mould Technology, School of Materials Science and Engineering, Huazhong University of Science and Technology, 1037 Luoyu Road, Wuhan 430074, China
[3] School of Materials Science and Engineering, Hebei University of Technology, Tianjin 300130, China
* Correspondence: lux@hust.edu.cn (X.L.); chyflian@hlju.edu.cn (Y.L.)

Abstract: Soot-containing terbium (Tb)-embedded fullerenes were prepared by evaporation of Tb_4O_7-doped graphite rods in an electric arc discharge chamber. After 1,2,4-trichlorobenzene extraction of the soot and rotary evaporation of the extract, a solid product was obtained and then dissolved into toluene by ultrasonication. Through a three-stage high-pressure liquid chromatographic (HPLC) process, Tb@C_{82} (I, II) isomers were isolated from the toluene solution of fullerenes and metallofullerenes. With the success of the growth of cocrystals of Tb@C_{82} (I, II) with Ni(OEP), the molecular structures of Tb@C_{82} (I) and Tb@C_{82} (II) were confirmed to be Tb@C_{2v}(9)-C_{82} and Tb@C_s(6)-C_{82}, respectively, based on crystallographic data from X-ray single-crystal diffraction. Moreover, it was found that Tb@C_{82} (I, II) isomers demonstrated different packing behaviors in their cocrystals with Ni(OEP). Tb@C_{2v}(9)-C_{82} forms a 1:1 cocrystal with Ni(OEP), in which Tb@C_{2v}(9)-C_{82} is aligned diagonally between the Ni(OEP) bilayers to form zigzag chains. In sharp contrast, Tb@C_s(6)-C_{82} forms a 2:2 cocrystal with Ni(OEP), in which Tb@C_s(6)-C_{82} forms a centrosymmetric dimer that is aligned linearly with Ni(OEP) pairs to form one-dimensional structures in the a–c lattice plane. In addition, the distance of a Ni atom in Ni(OEP) to the C_s(6)-C_{82} cage is much shorter than that to the C_{2v}(9)-C_{82} one, indicative of a stronger π-π interaction between Ni(OEP) and the C_{82} carbon cage in the cocrystal of Tb@C_S(6)-C_{82} and Ni(OEP). Density functional theory calculations reveal that the regionally selective dimerization of Tb@C_S(6)-C_{82} is the result of a dominant unpaired spin existing on a particular C atom of the C_S(6)-C_{82} cage.

Keywords: metallofullerene; terbium; cocrystals; centrosymmetric dimer; unpaired spin

Citation: Dong, W.; Zhou, Q.; Shen, W.; Yang, L.; Jin, P.; Lu, X.; Lian, Y. The Various Packing Structures of Tb@C_{82} (I, II) Isomers in Their Cocrystals with Ni(OEP). *Nanomaterials* **2023**, *13*, 994. https://doi.org/10.3390/nano13060994

Academic Editor: Werner Blau

Received: 17 February 2023
Revised: 5 March 2023
Accepted: 7 March 2023
Published: 9 March 2023

1. Introduction

Endohedral metallofullerenes (EMFs) are formed by embedding metal atoms or clusters of metal and nonmetal atoms inside the carbon cage of a fullerene molecule. Due to their unique molecular and electronic structures, EMFs are superior to fullerenes for their extensive applications in the fields of medical diagnostic and therapeutic reagents, organic photovoltaic power generation, organic superconductors, and single-molecule magnets [1–7]. To date, EMFs have been a hotspot for investigations of a series of novel nanocarbon materials.

Among the large number of EMFs, C_{82}-based mono-EMFs (M@C_{82}, M = encapsulated metal atom) are of particular interest due to their availability, solubility, and redox activity [8–10]. Based on the formal charge of the embedded metal atom, mono-EMFs can be classified as divalent group $M^{2+}@{C_{82}}^{2-}$ (M = Sm, Eu, Tm, Yb and alkaline earth metals) [11–15], trivalent group $M^{3+}@{C_{82}}^{3-}$ (M = Sc, Y, La, Ho, Ce, Pr, Nd, Gd, Dy, Er and Lu) [16–24], or tetravalent group $M^{4+}@{C_{82}}^{4-}$ (M = Th and U) [25,26]. Elucidation of the molecular and crystallographic structures of C_{82}-based mono-EMFs plays a crucial role for

understanding the interactions between encapsulated metal atoms and the C_{82} carbon cage, as well as the stability, growth mechanism, and packing behavior of M@C_{82} molecules.

As one of the rare earth elements, terbium is of special interest. On the one hand, terbium has variable valence states. As the starting material for the synthesis of EMFs, Tb_4O_7 is a mixture of oxides with two valence states of +3 and +4. Accordingly, study of Tb-containing mono-EMFs would be beneficial to clarify the electronegative nature of fullerene cages as well as the electronic structure of EMFs [27]. On the other hand, terbium is a well-known rare earth luminescent material, and its compounds have better performance in optical properties. Moreover, Tb_2@C_{80}(CH_2Ph), as a single molecular magnet demonstrates, has a very strong coercivity and the highest blocking temperature (28.9 K) of the di-nuclear lanthanide complexes [28]. Therefore, Tb-containing EMFs might be applicable in many fields as novel optical and magnetic materials.

Investigation of the molecular and crystalline structures of EMFs is fundamental for their potential applications. Previously, some Tb-containing clusterfullerenes, including Tb_3N@C_{2n}(2n = 80, 86 and 88) [29], TbCN@C_{82} [30], TbCN@C_{76} [31], and Tb_2C_2@C_{82} [32] have been successfully synthesized and separated, and their molecular and crystalline structures have been determined. It was reported for TbCN@C_{82} and TbCN@C_{76} that TbNC clusters are flexible, and the geometry of the embedded TbNC clusters and the length of the Tb-N(C)/C-N bond can be greatly changed by changing the size of the isomer or carbon cage structure. However, the crystalline structures of Tb-containing mono-EMFs have not been reported yet, even though some of them have been isolated and characterized electrochemically and spectroscopically [33,34].

On the other hand, with the successful preparation of cocrystals of mono-EMF and metal octaethylporphyrin M(OEP), the packing behaviors of some mono-EMFs have been clarified. Apart from the normal packing of individual mono-EMFs, the dimerization of some mono-EMFs, including Li@C_{60} [35], Y@C_s(6)-C_{82} [36], Er@C_s(6)-C_{82} [37], and Ce@C_{2v}(9)-C_{82} [38] occurs in their cocrystals with M(OEP). It was found that the formed dimers are linked by a single C–C interfullerene bond.

In this work, two isomers of Tb@C_{82} were isolated, and their cocrystals with Ni(OEP) were successfully prepared. Crystallographic characterization revealed that the molecular structures of Tb@C_{82} (I, II) could be separately described as Tb@C_{2v}(9)-C_{82} and Tb@C_S(6)-C_{82}, and that the labile isomer demonstrated a high degree of regioselective dimerization in its crystalline state. Theoretical calculations indicate that the varied anisotropy of the cage spin density, determined by carbon cage geometry and the metal center position, is responsible for the different packing behaviors of the two Tb@C_{82} (I, II) isomers.

2. Materials and Methods

2.1. Synthesis, Isolation and Characterization

Soot-containing Tb@C_{82} isomers were prepared by a modified arc discharge method. The anode was a graphite rod (Ø8 × 140 mm, Sinosteel Shanghai Carbon Plant, Shanghai, China) drilled with a hole (Ø6 × 120 mm) and filled with a powder mixture of Tb_4O_7 (Aladdin, Shanghai, China) and graphite (Tianjin Kermel Chemical Reagent Co.,Ltd, Tianjin, China) with a molar ratio Tb/C = 1:15, and the cathode was a graphite block (20 × 20 mm, Sinosteel Shanghai Carbon Plant Co., Ltd., Shanghai, China). Tb_4O_7 and graphite were the metal and carbon sources, respectively, for the formation of EMFs. An arc was generated under a He (Beijing AP Baif Gases Industry Co., Ltd., Beijing, China) atmosphere of 400 mbar at an electric current of 100 A. In comparison with the classical arc discharge method [39,40], a metal source of a higher oxidation state and a He atmosphere of a higher pressure were applied to the preparation of metallofullerenes, based on the optimization of the experimental conditions.

When the arc chamber had cooled to room temperature, the yielded soot was collected and then extracted with 1,2,4-trichlorobenzene (Aladdin, Shanghai, China) in a round-bottomed flask connected to a condenser at about 387 K for 12 h. After removal of 1,2,4-trichlorobenzene using a rotary evaporator, the residue powder was immediately re-

dissolved in the mixed solvent of CS_2/toluene (Tianjin City Guang Fu Tech. Development Co., Ltd., Tianjing, China) (1:5, *v*/*v*) under the action of ultrasonic waves. In comparison with toluene, carbon disulfide (CS_2, Aladdin, Shanghai, China) has better solubility toward EMFs and can be easily removed by rotary evaporation at room temperature. Thus, instead of pure toluene, the mixed solvent of CS_2/toluene was applied to the redissolution of fullerenes and EMFs.

The isolation of Tb@C_{82} (I, II) isomers was conducted on a recycling preparative high-performance liquid chromatograph (HPLC, LC-9104, Analytical Co., Ltd., Kyoto, Japan) using toluene as the eluent. Three columns, including 5PYE (25 × 250 mm, NacalaiTesque, Kyoto, Japan), Buckyprep-M (25 × 250 mm, NacalaiTesque, Kyoto, Japan), and Buckyprep (25 × 250 mm, NacalaiTesque, Kyoto, Japan), were applied in a three-stage separation procedure. The purity of isolated Tb@C_{82} (I, II) isomers was checked by analytical HPLC (L-2000, Hitachi, Tokyo, Japan) and a matrix-assisted laser desorption/ionization time-of-flight (MALDI-TOF) mass spectrometer (Biflex III, Bruker, Bremen, Germany). The analytical HPLC was carried out on a Buckyprep column (4.6 × 250 mm, NacalaiTesque, Kyoto, Japan), and the matrix for MALDI mass spectrometry was 1,1,4,4-tetraphenyl-1,3-butadiene (TPB, Aladdin, Shanghai, China).

The optical absorption spectra of the Tb@C_{82} (I, II) isomers were recorded by a UV750 spectrometer (Perkin Elmer LAMBDA, Waltham, MA, USA), with a CS_2 solution of Tb@C_{82} (I) or Tb@C_{82} (II) in a quartz cell (1 cm). Electrochemical measurements were by a CHI-660E (Chenhua Energy Co., Ltd., Shanghai, China) instrument in a conventional three-electrode cell consisting of a platinum plate working electrode, a platinum plate as the counter-electrode, and one Ag electrode as a reference electrode. O-dichlorobenzene (o-DCB, Aladdin, Shanghai, China) was treated with magnesium strips to remove oxygen and water from the solution. The CV and DPV measurements were performed in o-dichlorobenzene (o-DCB) containing tetra(n-butyl) ammonium hexafluorophosphate ((n-Bu)$_4$NPF$_6$), Aladdin, Shanghai, China) (0.05 M), with a scan rate of 20 mV·s^{-1} at room temperature. All redox potentials were recorded on the Ag reference electrode and corrected according to $Fc^{0/+}$.

2.2. Single-Crystal X-ray Diffraction Analysis

Ni(OEP) composed of C, Ni, H and N elements was applied as the cocrystal agent for the formation of cocrystals with Tb@C_{82} (I, II), in which Ni coordinates with porphyrin via four Ni-N coordinated bonds. The π-π interaction between Ni(OEP) (Aladdin, Shanghai, China) and Tb@C_{82} (I, II) makes it possible to grow cocrystals of Tb@C_{82} (I, II) and Ni(OEP). Benzene (Aladdin, Shanghai, China) and carbon disulfide are good solvents for Ni(OEP) and Tb@C_{82} (I, II), respectively, which could also crystallize with Ni(OEP) and Tb@C_{82} (I, II) to form cocrystals.

A slow solvent diffusion process was applied to the growth of cocrystals of Tb@C_{82} (I, II) isomers with Ni(OEP). A benzene solution of Ni(OEP) was put on a CS_2 solution of Tb@C_{2v}(9)-C_{82} or Tb@C_S(6)-C_{82} in a 5.0 mL centrifuge tube. After standing still at 275 K for 3 weeks in a refrigerator, black cocrystals appeared at the interface of benzene and CS_2, which were large enough for X-ray single-crystal diffraction analyses. The crystallographic data were collected on a diffractometer (D8 VENTURE, Bruker Analytik GmbH), and a multi-scan absorption correction was applied to the intensity data using the SADA program. For the cocrystal of Tb@C_{2v}(9)-C_{82} with Ni(OEP), the data were collected by a CCD collector at 173 K under a radiation wavelength of 0.65250 Å. In contrast, for the cocrystal of Tb@C_S(6)-C_{82} with Ni(OEP), the data were collected by a Photon100 CMOS collector at 100 K under a radiation wavelength of 0.88560 Å. The structures were solved using direct methods and refined by the SHELXL program. The crystallographic data for this paper can be found at CCDC1878018 and CCDC1878019, respectively.

2.3. Theoretical Calculation Details

Density functional theory (DFT) calculations were carried out using the M06-2X [41] functional in conjunction with the 6-31G* all-electron basis sets for the C [42,43] and

SDD [44] basis sets along with the corresponding relativistic small-core effective core potential for Tb (denoted as M06-2X/6-31G*~SDD). The DFT computations were calculated using the Gaussian 09 software package [45]. The results were visualized using the Mercury program [46].

3. Results and Discussion

3.1. Multistage HPLC Isolation of Tb@C_{82} (I, II) Isomers

Previously, pure endohedral metallofullerenes have been isolated by preparative high-performance liquid separation chromatography (HPLC) without exception, in which various columns are applied in a multi-stage procedure. In this work, Tb@C_{82} (I, II) isomers were isolated by the following process. The toluene solution of fullerenes and metallofullerenes was filtered with a 0.2 μm PTFE membrane, then subjected to three-stage HPLC isolation. Firstly, a 5PYE column was chosen to separate the mixture of fullerenes and metallofullerenes. The 5PYE was packed with planar aromatic 2-(1-pyrene)ethyl-group-modified silica gel, which is appropriate to separate fullerenes and metallofullerenes in line with their molecular weights. As shown in Figure 1a,b, the eluate collected at 32–39.5 min was mainly composed of C_{88} and Tb@C_{82} (I, II). Secondly, a Buckyprep-M column was adopted to separate C_{88} from Tb@C_{82} (I, II). The Buckyprep-M column was packed with phenothiazine-bonded silica gel, which plays a crucial role in isolating metallofullerenes from fullerenes. It can be seen in Figure 1c,d that the eluate collected at 33.5–40 min was mainly composed of Tb@C_{82} (I, II). Finally, the Tb@C_{82} (I, II) isomers were isolated on a Buckyprep column by cyclic HPLC. The Buckyprep column was packed with 3-(1-pyrene)propyl-bonded silica gel, which has good ability to isolate metallofullerene isomers. As displayed in Figure 1e, Tb@C_{82} (I) and Tb@C_{82} (II) were successfully isolated after five cycles.

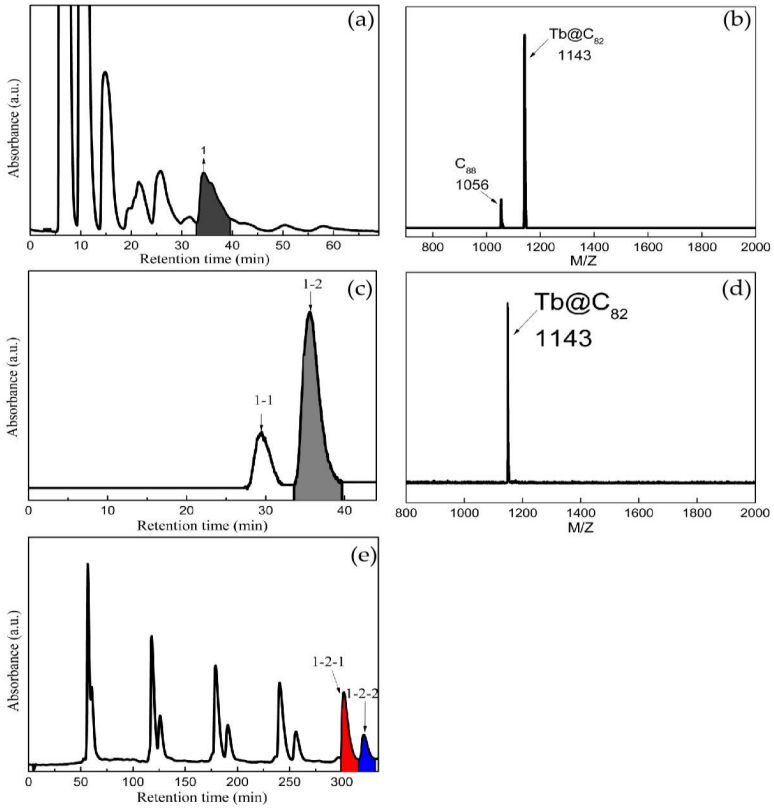

Figure 1. The (**a**) first, (**c**) second and (**e**) third stages of HPLC isolation of Tb@C_{82} (I, II) isomers (column size: ϕ20 mm × 250 mm; injection volume: 20 mL; eluent: toluene with a flow rate of 10 mL/min; detection wavelength: 290 nm at 298 K). The MALDI-TOF mass spectra of (**b**) fraction 1 and (**d**) fraction 1-2.

3.2. Purity Evaluation and Spectroscopic Characterization

The purity of the isolated Tb@C_{82} (I, II) samples was evaluated by analytical HPLC chromatograms and MALDI-TOF mass spectra. It can be seen in Figure 2a that the retention times of the Tb@C_{82} (I, II) isomers on the Buckyprep column are quite different, and the two isomers demonstrate a single HPLC peak with quite good symmetry, respectively. Shown in Figure 2b are the MALDI-TOF spectra of Tb@C_{82} (I, II), which demonstrate a single peak at m/z 1143, corresponding to the molecular mass of Tb@C_{82}. Moreover, the observed isotopic distributions agree very well with the corresponding theoretically calculated ones. Therefore, it is reasonable for us to conclude that the purity of the isolated Tb@C_{82} (I, II) isomers is more than 95%.

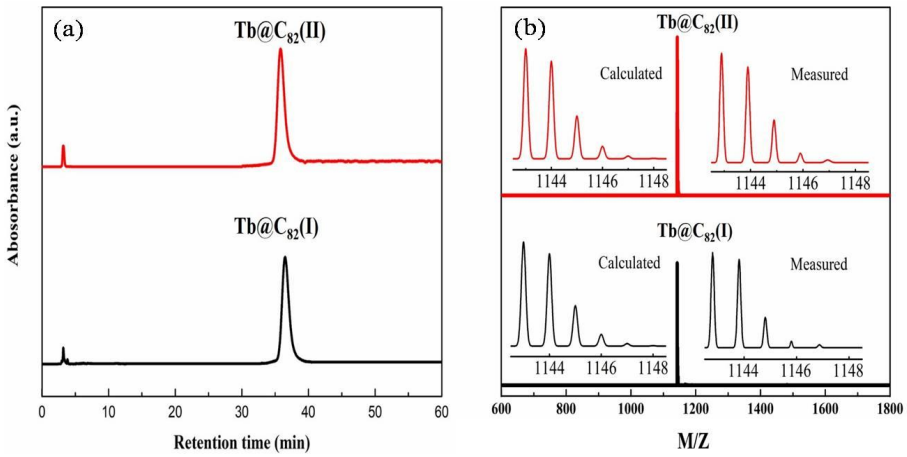

Figure 2. (**a**) Analytical liquid chromatography chromatograms on a Buckyprep column (Φ = 4.6 × 250 mm, 1 mL/min in toluene flow) and (**b**) MALDI-TOF mass spectra of Tb@C_{82} (I, II) isomers.

The vis-NIR absorption spectra of Tb@C_{82} (I, II) are shown in Figure 3. Tb@C_{82} (I) shows three distinct peaks at 635, 998, and 1413 nm, and two characteristic peaks at 780 and 1089 nm are identified for Tb@C_{82} (II). The visible and NIR absorption features of EMFs are owing to the π-π* transitions of the fullerene cages, which are directly relate to the symmetry and charge state of the carbon cages. Therefore, information on the symmetry of the carbon cages could be extracted from the optical absorption spectroscopy of EMFs. The vis-NIR absorption spectra of Tb@C_{2v}(9)-C_{82} and Tb@C_S(6)-C_{82} are substantially similar to these of Y@C_{2v}(9)-C_{82} and Y@C_S(6)-C_{82}, whose molecular structures have been determined by X-ray single-crystal diffraction [36]. Accordingly, the carbon cages of Tb@C_{82} (I) and Tb@C_{82} (II) are tentatively ascribed to C_{2v} and C_S symmetries, and the oxidation state of the endohedral Tb atom might be +3.

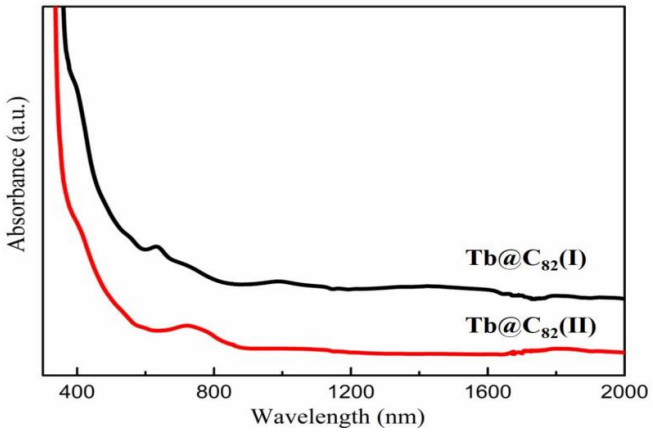

Figure 3. The vis-NIR absorption spectra of Tb@C_{82} (I, II) isomers in CS_2 at 298 K.

3.3. Crystallographic Study

In line with the crystallographic data and structural refinement statistics of the cocrystals obtained in this work (Table S2), Tb@C_{82} (I) crystallizes with Ni(OEP) in the common *C2/m* space group, and a pair of disordered C_{2v}-C_{82} cages can be identified. Among them, half of the Ni(OEP) molecule and both halves of the C_{82} cage are located on one side of the lens plane in the asymmetric unit, and the equal phase occupancies are 0.5. Tb@$C_S(6)$-C_{82} isomers crystallized in the commonly encountered space group $P2_{1/c}$. Both cocrystals belong to a monoclinic crystal system, and based their crystallographic mirror planes, are not consistent with any symmetrical elements of the C_{82} cages.

The molecular structures of the two Tb@C_{82} isomers were unambiguously determined by means of single-crystal XRD. As shown in Figure 4a, the fullerene cage of Tb@C_{82} (I) is clearly ascribed to $C_{2v}(9)$-C_{82}. Inside the cage, the Tb atom shows three disordered positions with fractional occupancy values of 0.6722 (Tb1), 0.2222 (Tb2), and 0.1056 (Tb3), respectively, indicative of a motional behavior (see Figure S2). Moreover, all of these metal positions are off the center of the carbon cage to some extent. The major metal atom (Tb1) resides near a [6,6]-bond (C47-C48), and the shortest terbium–cage distances are 2.313 Å for Tb to C47 and 2.308 Å for Tb to C48 (see Figure 5a). Contrastingly, the fullerene cage of Tb@C_{82} (II) is definitely assigned to $C_S(6)$-C_{82}, in which four disordered positions of the embedded Tb atom are identified with fractional occupancy values of 0.1069 (Tb1), 0.7951 (Tb2), 0.0499 (Tb3), and 0.0484 (Tb4), respectively (see Figure S2), in sharp contrast to the fixed positions of Y^{3+} and Er^{3+} inside $C_S(6)$-C_{82} observed in their corresponding cocrystals with Ni(OEP) [36,37]. The major Tb (Tb2) resides opposite a pentagon−hexagon−hexagon junction, and the shortest metal–cage distance is 2.288 Å for Tb2 to C65 (see Figure 5b), which is a little bit shorter than that observed in $C_{2v}(9)$-C_{82}. Moreover, it can be seen from Figure 4b that two Tb@$C_S(6)$-C_{82} molecules are linked via a C−C bond whose bond length is 1.624 Å, and a dimeric structure is formed similar to the dimers of Y@$C_S(6)$-C_{82} and Er@$C_S(6)$-C_{82} discovered in their corresponding cocrystals with Ni(OEP). In addition, the Tb@$C_S(6)$-C_{82} molecules adopt an orientation in the dimer to keep the encaged Tb atoms as far away as possible.

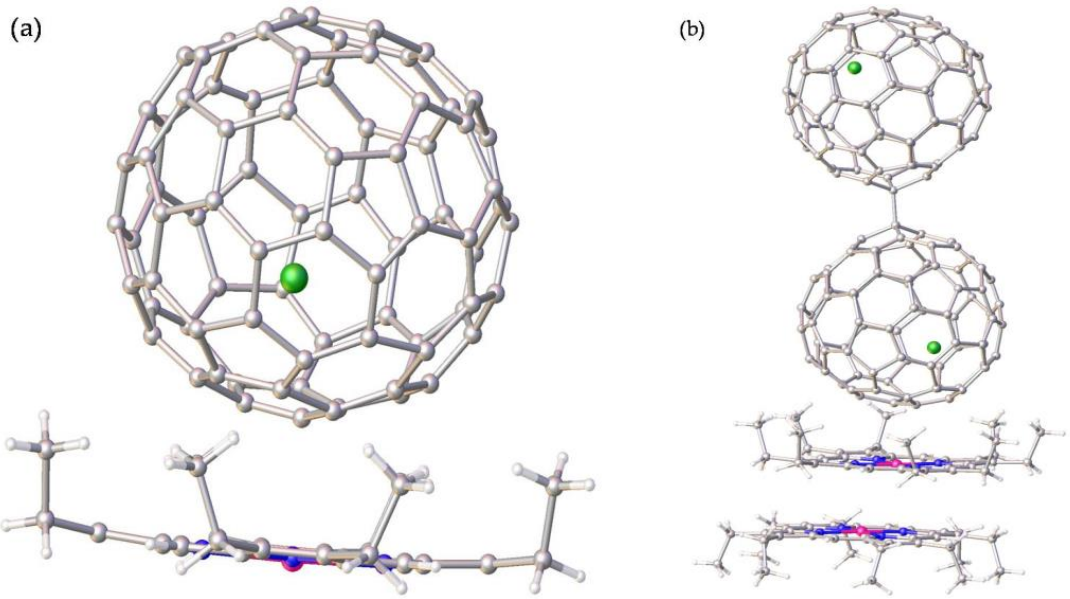

Figure 4. The orientations of (**a**) Tb@$C_{2v}(9)$-C_{82} and (**b**) Tb@$C_S(6)$-C_{82} to Ni(OEP) in the cocrystals of Tb@$C_{2v}(9)$-C_{82}]·[Ni(OEP)] and 2[Tb@$C_S(6)$-C_{82}]·2[Ni(OEP)], respectively. Only the major Tb site and one carbon cage orientation are shown. Solvent molecules and H atoms are omitted for clarity.

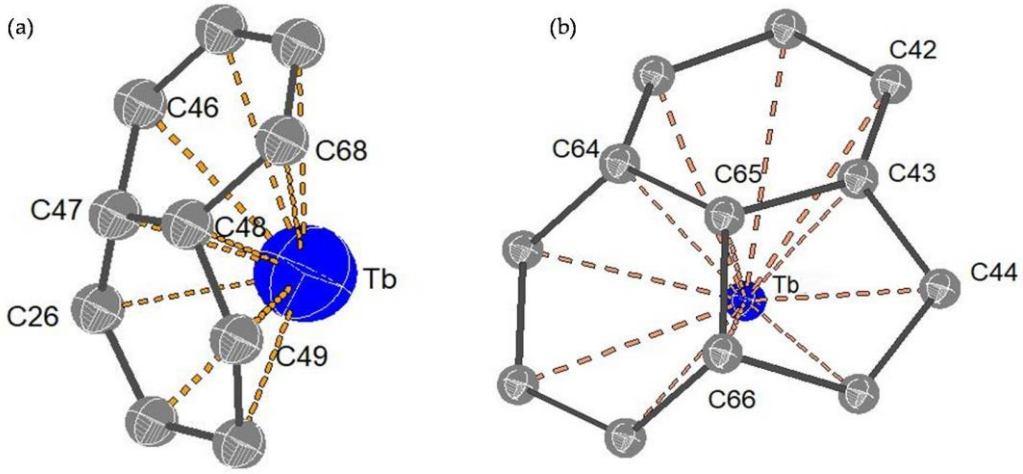

Figure 5. The interaction of the metal cation (major metal site) with the nearest cage carbon atoms for (**a**) Tb@C_{2v}(9)-C_{82} and (**b**) Tb@C_S(6)-C_{82}.

Figure 6 depicts the packing structures of the two cocrystals of isomeric Tb@C_{82} (I, II) and Ni(OEP). It can be seen in Figure 6a that monomeric Tb@C_{2v}(9)-C_{82} molecules form zigzag chains in this polymorph, while Ni(OEP) molecules are aligned in two dimensions, forming a closely packed bilayer with a gap of 3.1122 Å. The Tb@C_{2v}(9)-C_{82} molecule chains pack closely between the Ni(OEP) bilayers, which are placed 20.7846 Å apart. In contrast, as indicated in Figure 6b, the Ni(OEP) bilayers placed 23.7195 Å apart do not align in two-dimensional planes and dimerization occurs for Tb@C_S(6)-C_{82} molecules in the cocrystal of Tb@C_S(6)-C_{82} and Ni(OEP), similar to the arrangement of Y@C_S(6)-C_{82} and Er@C_S(6)-C_{82} in their corresponding cocrystals with Ni(OEP) [36,37]. Of interest to note is that the gap in the Ni(OEP) bilayer (3.184 Å) is larger but the distance between Ni(OEP) and the carbon cage (2.861 Å) is shorter than those observed in Figure 6a. Thus, a weaker π-π interaction in the Ni(OEP) bilayers and a stronger π-π interaction between Ni(OEP) and the carbon cage are expected in the cocrystal of Tb@C_S(6)-C_{82} and Ni(OEP) [47].

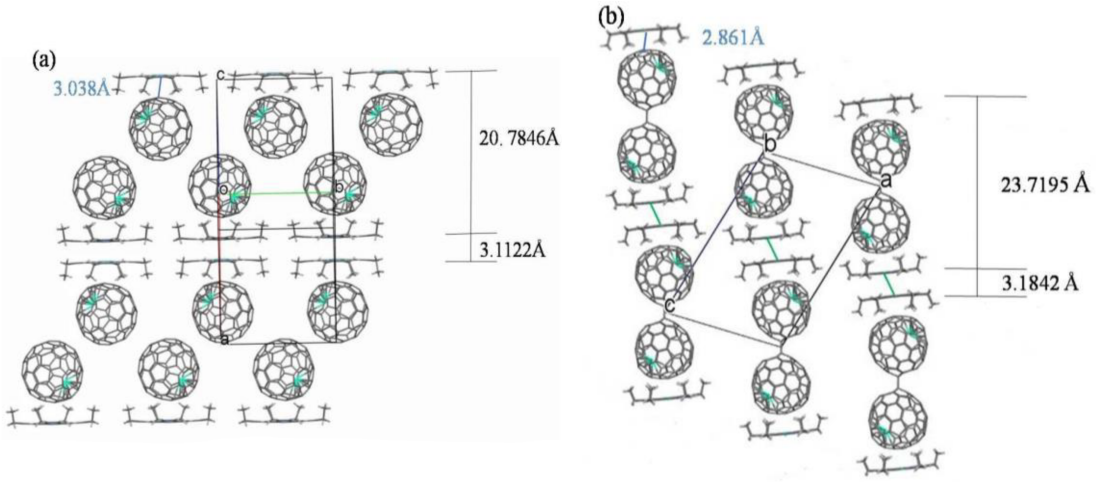

Figure 6. The packing structures of (**a**) Tb@C_{2v}(9)-C_{82} and (**b**) Tb@C_S(6)-C_{82} in their cocrystals with Ni(OEP). Only one cage orientation and the major terbium site are illustrated, with solvent molecules omitted for clarity.

3.4. Computational Study

DFT calculations at the M06-2X/6-31G*~SDD level of theory were then carried out to understand the different packing behaviors of the two Tb@C_{82} isomers. According to the electronic configuration of element Tb[Xe]$4f^9 6s^2$ and its formal charge of 3+, different spin

multiplicities were considered for each Tb@C_{82} isomer during the geometric optimization. Table S1 shows that Tb@C_S(6)-C_{82} and Tb@C_{2v}(9)-C_{82} both have open-shell electronic structures due to the presence of odd electrons, but they energetically prefer the sextet and octet electronic states as their ground states, respectively.

Electrons could be spin-up and -down while distributing on an orbital, which are marked as α and β spin states, respectively. Spin density reflects the difference in the density distributions of α and β spin electrons in an open-shell system. In contrast, the spin density is zero for a closed-shell system at ground state because the α and β spin electrons are equal. The quantitative calculations give the electron spin density of a molecule. The larger the absolute value of spin density is, the more single electrons there are after spatial integration, the more chances there are for the whole cluster system to lose or gain electrons, and the more active the system. The electron spin density obtained by calculation helps to interpret the experimental data. With accurate theory, calculated electron spin density can even verify or predict experimental results.

To rationalize the experimental results, the spin-density distributions of Tb@C_S(6)-C_{82} and Tb@C_{2v}(9)-C_{82} were then calculated and compared (Figure 7). The spin density was the largest (ca. 6 a.u.) at the internal Tb^{3+} cation due to its $4f^8$ electronic configuration (six unpaired electrons according to Hund's rule), since the Tb atom donates one 4f and two 6s electrons to the outer C_{82} cage. After accepting the three electrons from Tb, the $C_{82}{}^{3-}$ cage has an unpaired electron and thus also has an obvious spin-density distribution. Remarkably, C44 on the Tb@C_S(6)-C_{82} surface exhibits the largest spin-density value (−0.22 a.u.) among the cage carbon atoms, indicating that it is an ideal site for the exohedral dimerization reaction to achieve spin pairing between two monomers. Indeed, our experiment shows that exactly this reaction site is involved during the dimer formation. A similar situation exists in Y@C_S(6)-C_{82} and Er@C_S(6)-C_{82}, in which the carbon atoms at the site of dimerization also possess the highest spin-density value [36,37]. As for Tb@C_{2v}(9)-C_{82}, however, all the carbon atoms have moderate spin density, suggesting their low reactivity. Therefore, the different dimerization behaviors between Tb@C_S(6)-C_{82} and Tb@C_{2v}(9)-C_{82} under the same crystallization conditions should be attributed to their rather different spin-density distributions on their C_{82} cages.

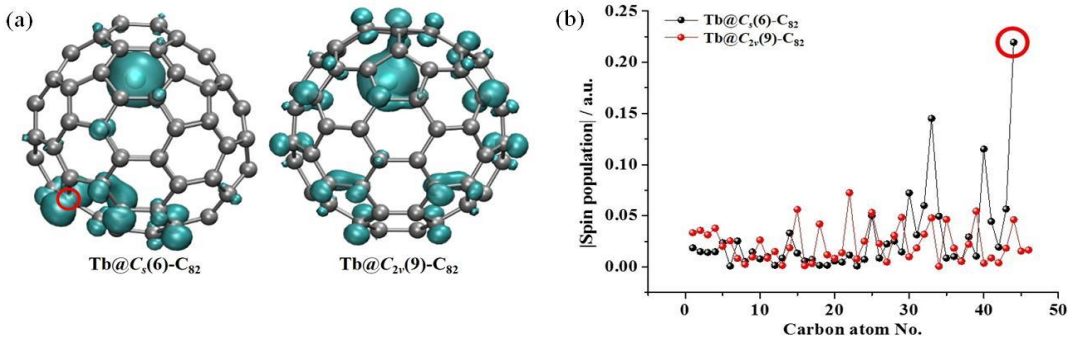

Figure 7. (**a**) Visualized spin density distributions and (**b**) corresponding spin population values of unequivalent cage carbon atoms of Tb@C_S(6)-C_{82} and Tb@C_{2v}(9)-C_{82}. The absolute values are used for easy comparison. Please refer to Figure S3 for the numbering schemes. The C44 site of Tb@C_S(6)-C_{82}, with the largest spin density among all cage carbons, is highlighted by the red circle.

3.5. Electrochemical Study

The redox properties of Tb@C_{2v}(9)-C_{82} and Tb@C_S(6)-C_{82} were investigated by cyclic voltammetry (CV) and differential pulse voltammetry (DPV, see Figure S4). It can be seen in Figure 8 that both Tb@C_{2v}(9)-C_{82} and Tb@C_S(6)-C_{82} display two oxidation and five reduction DPV peaks, whose corresponding potentials are listed in Table 1. In comparison with those reported for M@C_{82} (I, II) (M = Y [36], Er [37], and Nd [48]), the redox potentials obtained here for Tb@C_{82} (I, II) largely enrich the electrochemistry of C_{82}-based mono-EMFs. Since both the first oxidation and first reduction potentials of Tb@C_S(6)-C_{82} are lower

than those of Tb@C_{2v}(9)-C_{82}, respectively, it is concluded that the former is accordingly more easily oxidized or reduced than the latter. Moreover, the electrochemical band gaps ($\Delta E = E_{1/2,\ ox}{}^{(1)}$-$E_{1/2,\ red}{}^{(1)}$) of Tb@$C_{2v}$(9)-$C_{82}$ and Tb@C_S(6)-C_{82} are calculated to be 0.49 and 0.37 V, respectively, confirming that the thermodynamic stability of Tb@C_{2v}(9)-C_{82} is higher than that of Tb@C_S(6)-C_{82}.

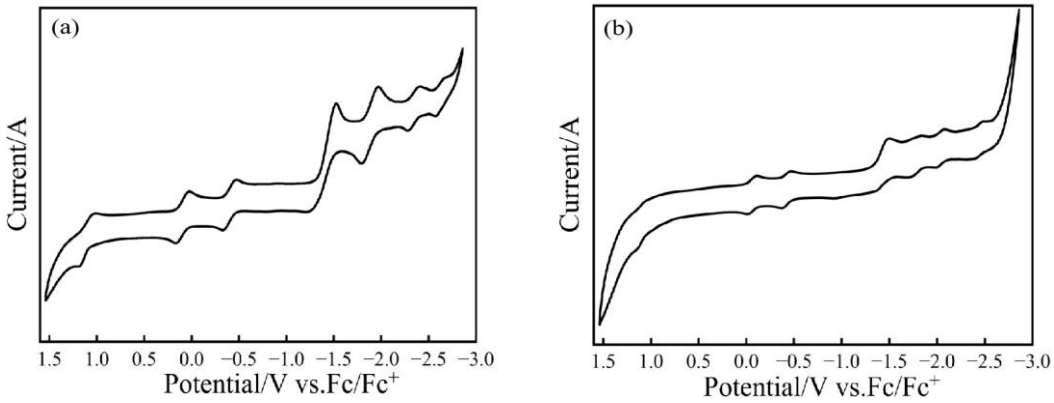

Figure 8. CV curves of (**a**) Tb@C_{2v}(9)-C_{82} and (**b**) Tb@C_S(6)-C_{82} isomers. Conditions: working electrode, platinum plate; counter electrode, platinum plate; reference electrode, Ag wire; supporting electrolyte, 0.05 M n-Bu_4NPF_6 in o-dichlorobenzene; scan rate, 20 mV/s.

Table 1. Redox Potentials (V vs. Fc/Fc^+) [a] of Tb@C_{2v}(9)-C_{82} and Tb@C_S(6)-C_{82}.

EMFs	$^{ox}E_2$ (V)	$^{ox}E_1$ (V)	$^{red}E_1$ (V)	$^{red}E_2$ (V)	$^{red}E_3$ (V)	$^{red}E_4$ (V)	$^{red}E_5$ (V)	EC Gap (V)
Tb@C_{2v}(9)-C_{82}	1.10	0.09	−0.40	−1.36	−1.87	−2.34	−2.61	0.49
Tb@C_S(6)-C_{82}	1.10	−0.05	−0.42	−1.43	−1.76	−2.04	−2.43	0.37

[a] Half-wave potentials in o-DCB unless otherwise addressed.

4. Conclusions

In summary, two Tb@C_{82} (I, II) isomers were isolated by multi-stage preparative high-performance liquid chromatography (HPLC). Optical absorption spectra indicate that the carbon cages of Tb@C_{82} (I, II) are of C_{2v} and C_S symmetry, respectively, and the formal oxidation state of endohedral Tb cation is +3. Electrochemical studies evidence that the thermodynamic stability of Tb@C_{2v}(9)-C_{82} is higher than that of Tb@C_S(6)-C_{82}. With the successful growth of cocrystals of Tb@C_{82} (I, II) with Ni(OEP), the various C_{2v} and C_S symmetries of carbon cages as well as the disordered sites of endohedral Tb cations were explicitly determined by crystallographic study. Moreover, in their corresponding cocrystals with Ni(OEP), Tb@C_S(6)-C_{82} molecules form dimers via a covalent C-C bond, while monomeric Tb@C_{2v}(9)-C_{82} molecules assemble into a zig-zag chain. DFT calculations suggest that a specific cage carbon atom with an abnormally high spin density is responsible for the regioselective dimerization of Tb@C_S(6)-C_{82} molecules.

Supplementary Materials: The following supporting information can be downloaded at https://www.mdpi.com/article/10.3390/nano13060994/s1: soot preparation; DPV characterization; MALDI-TOF mass spectrum of the TCB extract (Figure S1); positions of the disordered terbium atoms in (a) Tb@C_{2v}(9)-C_{82} and (b) Tb@C_S(6)-C_{82} with respect to C_{82} cage orientation, respectively (Figure S2); relative energies (kcal/mol) of Tb@C_S(6)-C_{82} and Tb@C_{2v}(9)-C_{82} with different spin multiplicities (Table S1); numbering scheme of the unequivalent cage carbon atoms in (a) Tb@C_S(6)-C_{82} and (b) Tb@C_{2v}(9)-C_{82} (Figure S3); DPV curves of Tb@C_{2v}(9)-C_{82} and (b) Tb@C_S(6)-C_{82} (Figure S4); the crystallographic data of [Tb@C_{2v}(9)-C_{82}]·[Ni(OEP)]·2(C_6H_6) and 2[Tb@C_S(6)-C_{82}]·2[Ni(OEP)]·2(C_6H_6)·(CS_2) (Table S2).

Author Contributions: Conceptualization, W.D. and Y.L.; methodology, W.D., Q.Z., and W.S.; software, L.Y. and P.J.; validation, W.D., Q.Z., W.S., and L.Y.; investigation, W.D. and Q.Z.; resources, Y.L. and X.L.; data curation, W.D. and W.S.; writing—original draft preparation, W.D.; writing—review and editing, Y.L.; visualization, W.D. and L.Y.; supervision, Y.L. and X.L.; funding acquisition, Y.L. and X.L. All authors have read and agreed to the published version of the manuscript.

Funding: This research was funded by basic research funds for colleges and universities in Heilongjiang Province, grant number 2022-KYYWF-1064.

Data Availability Statement: CCDC1878018 and CCDC1878019 contain the supplementary crystallographic data for this paper. These data can be obtained free of charge via https://www.ccdc.cam.ac.uk/structures/ (accessed on 3 February 2022), or by emailing data_request@ccdc.cam.ac.uk, or by contacting The Cambridge Crystallographic Data Centre, 12 Union Road, Cambridge CB2 1EZ, UK; fax: +44 1223336033.

Conflicts of Interest: The authors declare no conflict of interest.

References

1. Chaur, M.N.; Melin, F.; Ortiz, A.L.; Echegoyen, L. Chemical, electrochemical, and structural properties of endohedral metallofullerenes. *Angew. Chem. Int. Ed.* **2009**, *48*, 7514–7538. [CrossRef] [PubMed]
2. Han, X.Y.; Xin, J.P.; Yao, Y.R.; Liang, Z.H.; Qiu, Y.F.; Chen, M.Q.; Yang, S.F. Capturing the long-sought Dy@C_{2v}(5)-C_{80} via benzyl radical stabilization. *Nanomaterials* **2022**, *12*, 3291–3301. [CrossRef]
3. Ubasart, E.; Borodin, O.; Fuertes-Espinosa, C.; Xu, Y.; García-Simón, C.; Gómez, L.; Juanhuix, J.; Gándara, F.; Imaz, I.; Maspoch, D.; et al. Three-shell supramolecular complex enables the symmetry-mismatched chemo- and regioselective bis-functionalization of C_{60}. *Nat. Chem.* **2021**, *13*, 420–427. [CrossRef] [PubMed]
4. Ksenofontov, A.A.; Bichan, N.G.; Ilya, A.K.; Elena, V.A.; Mikhail, B.B.; Anatolij, I.V. Novel non-covalent supramolecular systems based on zinc(II) bis(dipyrromethenate)s with fullerenes. *J. Mol. Liq.* **2018**, *269*, 327–334. [CrossRef]
5. Wei, G.; Fan, B.B.; Qi, F.; Lin, F.R.; Sun, R.; Xia, X.X.; Gao, J.H.; Zhong, C.; Lu, X.H.; Min, J.; et al. Asymmetric isomer effects in benzo [c][1,2,5] thiadiazole-fused nonacyclic acceptors: Dielectric constant and molecular crystallinity control for significant photovoltaic performance enhancement. *Adv. Funct. Mater.* **2021**, *31*, 2104369.
6. Alexander, A.K.; Mikhail, M.L.; Nataliya, G.B.; Ilya, A.K.; Nadezhda, O.K.; Ksenia, V.K.; Elena, V.A. Non-covalent supramolecular systems with photoinduced electron transfer based on zinc bis(dipyrromethenate)s and C_{60}. *Dyes Pigm.* **2021**, *185*, 108918.
7. Shi, W.S.; Salerno, F.; Ward, M.D.; Santana-Bonilla, A.; Wade, J.; Hou, X.; Liu, T.; Dennis, T.J.; Campbell, A.J.; Jelfs, K.E.; et al. Fullerene desymmetrization as a means to achieve single-enantiomer Eelectron acceptors with maximized chiroptical responsiveness. *Adv. Mater.* **2021**, *33*, 2004115. [CrossRef]
8. Lu, X.; Akasaka, T.; Nagase, S. Chemistry of endohedral metallofullerenes: The role of metals. *Chem. Commun.* **2011**, *47*, 5942–5957. [CrossRef]
9. Rodríguez-Fortea, A.; Balch, A.L.; Poblet, J.M. Endohedral metallofullerenes: A unique host–guest association. *Chem. Soc. Rev.* **2011**, *40*, 3551–3563. [CrossRef]
10. Suzuki, T.; Kikuchi, K.; Oguri, F.; Nakao, Y.; Suzuki, S.; Achiba, Y.; Yamamoto, K.; Funasaka, H.; Takahashi, T. Electrochemical properties of fullerenolanthanides. *Tetrahedron* **1996**, *52*, 4973–4982. [CrossRef]
11. Xu, W.; Niu, B.; Feng, L.; Shi, Z.J.; Lian, Y.F. Access to an unexplored chiral C_{82} cage by encaging a divalent metal: Structural elucidation and electrochemical studies of Sm@C_2(5)-C_{82}. *Chem. Eur. J.* **2012**, *18*, 14246–14249. [CrossRef]
12. Hu, Z.; Hao, Y.; Slanina, Z.; Gu, Z.G.; Shi, Z.J.; Uhlík, F.; Zhao, Y.F.; Feng, L. Popular C_{82} fullerene cage encapsulating a divalent metal ion Sm^{2+}: Structure and electrochemistry. *Inorg. Chem.* **2015**, *54*, 2103–2108. [CrossRef]
13. Bao, L.P.; Yu, P.Y.; Li, Y.; Pan, C.W.; Shen, W.Q.; Jin, P.; Liang, S.Q.; Lu, X. Highly regioselective complexation of tungsten with Eu@C_{82}/Eu@C_{84}: Interplay between endohedral and exohedral metallic units induced by electron transfer. *Chem. Sci.* **2019**, *10*, 4945–4950. [CrossRef] [PubMed]
14. Lu, X.; Slanina, Z.; Akasaka, T.; Tsuchiya, T.; Mizorogi, N.; Nagase, S. Yb@C_{2n} (n = 40, 41, 42): New fullerene allotropes with unexplored electrochemical properties. *J. Am. Chem. Soc.* **2010**, *132*, 5896–5905. [CrossRef]
15. Sado, Y.; Aoyagi, S.; Kitaura, R.; Miyata, Y.; Nishibori, E.; Sawa, H.; Sugimoto, K.; Shinohara, H. Structure of Tm@C_{82}(I) metallofullerene by single-crystal X-ray diffraction using the 1:2 co-crystal with octaethylporphyrinnickel (Ni(OEP)). *J. Phys. Chem. C* **2013**, *117*, 6437–6442. [CrossRef]
16. Iiduka, Y.; Wakahara, T.; Nakajima, K.; Nakahodo, T.; Tsuchiya, T.; Maeda, Y.; Akasaka, T.; Yoza, K.; Liu, T.H.; Mizorogi, N.; et al. Experimental and theoretical studies of the scandium carbide endohedral metallofullerene Sc_2C_2@C_{82} and its carbene derivative. *Angew. Chem. Int. Ed.* **2007**, *46*, 5562–5564. [CrossRef]
17. Wang, Z.; Nakanishi, Y.; Noda, S.; Niwa, H.; Zhang, J.Y.; Kitaura, R.; Shinohara, H. Missing small-bandgap metallofullerenes: Their isolation and electronic properties. *Angew. Chem. Int. Ed.* **2013**, *125*, 11986–11990. [CrossRef]
18. Akasaka, T.; Kono, T.S.; Matsunaga, Y.; Wakahara, T.; Nakahodo, T.; Ishitsuka, M.O.; Maeda, Y.; Tsuchiya, T.; Kato, T.; Liu, T.H.; et al. Isolation and characterization of carbene derivatives of La@C_{82}(Cs). *J. Phys. Chem. A* **2008**, *112*, 1294–1297. [CrossRef]

19. Slanina, Z.; Uhlík, F.; Feng, L.; Adamowicz, Z. Ho@C_{82} metallofullerene: Calculated isomeric composition. *ECS J. Solid State Sci. Technol.* **2022**, *11*, 5–8. [CrossRef]
20. Ding, J.Q.; Yang, S.H. Isolation and characterization of Pr@C_{82} and Pr_2@C_{80}. *J. Am. Chem. Soc.* **1996**, *118*, 11254–11257. [CrossRef]
21. Zhang, K.; Wang, C.; Zhang, M.; Bai, Z.; Xie, F.F.; Tan, Y.Z.; Guo, Y.; Hu, K.J.; Cao, L.; Zhang, S.; et al. A Gd@C_{82} single-molecule electrets. *Nat. Nanotechnol.* **2020**, *15*, 1019–1024. [CrossRef]
22. Nakanishi, Y.; Omachi, H.; Matsuura, S.; Miyata, Y.; Kitaura, R.; Segawa, Y.; Itami, K.; Shinohara, H. Size-selective complexation and extraction of endohedral metallofullerenes with cycloparaphenylene. *Angew. Chem. Int. Ed.* **2014**, *53*, 3102–3106. [CrossRef]
23. Fan, L.Z.; Yang, S.F.; Yang, S.H. Electrochemistry of metallofullerene films: The major isomer of Dy@C_{82}. *Chem. Eur. J.* **2003**, *9*, 5610–5617. [CrossRef]
24. Wang, J.; Zhao, Y.Y.; Lee, P.H.; Irle, S. Er^{3+} photoluminescence in Er_2@C_{82} and Er_2C_2@C_{82} metallofullerenes elucidated by density functional theory. *Inorg. Chem.* **2017**, *56*, 6576–6583. [CrossRef]
25. Wang, Y.F.; Morales-Martinez, R.; Zhan, X.X.; Yang, W.; Wang, Y.X.; Rodriguez-Fortea, A.; Poblet, J.M.; Feng, L.; Wang, S.; Chen, N. Unique four-electron metalto cage charge cransfer of Th to a C_{82} fullerene cage: Complete structural characterization of Th@C_{3v}(8)-C_{82}. *J. Am. Chem. Soc.* **2017**, *139*, 5110–5116. [CrossRef]
26. Yao, Y.R.; Rosello, Y.; Ma, L.; Santiago, A.R.P.; Metta-Magana, A.; Chen, N.; Rodriguez-Fortea, A.; Poblet, J.M.; Echegoyen, L. Crystallographic characterization of U@C_{2n} (2n = 82–86): Insights about metal-cage interactions for mono-metallofullerenes. *J. Am. Chem. Soc.* **2021**, *143*, 15309–15318. [CrossRef]
27. Yasutake, Y.; Shi, Z.; Okazaki, T.; Shinohara, H.; Majima, Y. Single molecular orientation switching of an endohedral metallofullerene. *Nano Lett.* **2005**, *5*, 1057–1060. [CrossRef]
28. Liu, F.P.; Velkos, G.; Krylov, D.S.; Spree, L.; Zalibera, M.R.; Samoylova, N.A.; Chen, C.H.; Rosenkranz, M.; Schiemenz, S.; Ziegs, F.; et al. Air-stable redox-active nanomagnets with lanthanide spins radical-bridged by a metal–metal bond. *Nat. Commun.* **2019**, *10*, 571–582. [CrossRef]
29. Tianming, Z.; Christine, M.B.; James, C.D.; Anne, C.; Harry, C.D.; Marilyn, M.O.; Alan, L.B. Isolation and structural characterization of a family of endohedral fullerenes including the large, chiral cage fullerenes Tb_3N@C_{88} and Tb_3N@C_{86} as well as the I_h and D_{5h} isomers of Tb_3N@C_{80}. *J. Am. Chem. Soc.* **2007**, *129*, 2035–2043.
30. Liu, F.F.; Wang, S.; Guan, J.; Wei, T.; Zeng, M.; Yang, S.F. Putting a terbium-monometallic cyanide cluster into the C_{82} fullerene cage: TbCN@C_2(5)-C_{82}. *Inorg. Chem.* **2014**, *53*, 5201–5205. [CrossRef]
31. Liu, F.F.; Wang, S.; Gao, C.L.; Deng, Q.M.; Zhu, X.J.; Kostanyan, A.; Westerström, R.; Jin, F.; Xie, S.Y.; Popov, A.A.; et al. Mononuclear clusterfullerene single-molecule magnet containing strained fused-pentagons stabilized by a nearly linear metal cyanide cluster. *Angew. Chem. Int. Ed.* **2017**, *56*, 1830–1834. [CrossRef] [PubMed]
32. Liu, F.F.; Wei, T.; Wang, S.; Guan, J.; Lu, X.; Yang, S.F. A bent Tb_2C_2 cluster encaged in a C_S(6)-C_{82} cage: Synthesis, isolation and X-ray crystallographic study. *Fuller. Nanotubes Carbon Nanostruct.* **2014**, *22*, 215–226. [CrossRef]
33. Feng, L.; Zhang, X.; Yu, Z.; Wang, J.; Gu, Z. Chemical modification of Tb@C_{82} by copper (I)-catalyzed cycloadditions. *Chem. Mater.* **2002**, *14*, 4021–4022. [CrossRef]
34. Dong, W.; Nie, M.S.; Lian, Y.F. Isolation and electrochemical property of Tb@C_{82} isomers. *Acta Chim. Sin.* **2017**, *75*, 453–456. [CrossRef]
35. Ueno, H.; Aoyagi, S.; Yamazaki, Y.; Ohkubo, K.; Ikuma, N.; Okada, H.; Kato, T.; Matsuo, Y.; Fukuzumi, S.; Kokubo, K. Electrochemical reduction of cationic Li^+@C_{60} toneutral Li^+@C_{60}: Isolation and characterization of endohedral [60] fulleride. *Chem. Sci.* **2016**, *7*, 5770–5774. [CrossRef]
36. Bao, L.; Pan, C.; Slanina, Z.; Uhlik, F.; Akasaka, T.; Lu, X. Isolation and crystallographic characterization of the labile isomer of Y@C_{82} cocrystallized with Ni(OEP): Unprecedented dimerization of pristine metallofullerenes. *Angew. Chem. Int. Ed.* **2016**, *55*, 9234–9238. [CrossRef]
37. Hu, S.F.; Liu, T.; Shen, W.Q.; Slanina, Z.; Akasaka, T.; Xie, Y.P.; Uhlik, F.; Huang, W.H.; Lu, X. Isolation and structural characterization of Er@C_{2v}(9)-C_{82} and Er@Cs(6)-C_{82}: Regioselective dimerization of a pristine endohedral metallofullerene induced by cage symmetry. *Inorg. Chem.* **2019**, *58*, 2177–2182. [CrossRef]
38. Suzuki, M.; Yamada, M.; Maeda, Y.; Sato, S.; Takano, Y.; Uhlik, F.; Slanina, Z.; Lian, Y.F.; Lu, X.; Nagase, S.; et al. The unanticipated dimerization of Ce@C_{2v}(9)-C_{82} upon co-crystallization with Ni(octaethylporphyrin) and comparison with monomeric M@C_{2v}(9)-C_{82} (M = La, Sc, and Y). *Chem. Eur. J.* **2016**, *22*, 18115–18122. [CrossRef]
39. Krätschmer, W.; Lowell, D.L.; Konstantinos, F.; Donald, R.H. Solid C_{60}: A new form of carbon. *Nature* **1990**, *347*, 354–358. [CrossRef]
40. Grigory, N.C.; Krätschmer, W.; Irina, V.O.; Gariy, A.G.; Natalia, G.V.; Kolonenko, A.L.; Aleksander, I.D. Synthesis of fullerenes in a high-frequency arc plasma under elevated helium pressure. *Carbon* **2013**, *62*, 389–392.
41. Zhao, Y.; Truhlar, D.G. The M06 suite of density functionals for main group thermochemistry, thermochemical kinetics, noncovalent interactions, excited states, and transition elements: Two new functionals and systematic testing of four M06-class functionals and 12 other functionals. *Theor. Chem. Acc.* **2008**, *120*, 215–241.
42. Petersson, G.A.; Al Laham, M.A.A. Complete basis set model chemistry. II. Open-shell systems and the total energies of the first-row atoms. *J. Chem. Phys.* **1991**, *94*, 6081–6090. [CrossRef]
43. Petersson, G.A.; Bennett, A.; Tensfeldt, T.G.; Al-Laham, M.A.; Shirley, W.A.; Mantzaris, J.A. Complete basis set model chemistry. I. The total energies of closed-shell atoms and hydrides of the first-row elements. *J. Chem. Phys.* **1988**, *89*, 2193–2218. [CrossRef]

44. Cao, X.; Dolg, M. Segmented contraction scheme for small-core lanthanide pseudopotential basis sets. *J. Mol. Struct. THEOCHEM* **2002**, *581*, 139–147. [CrossRef]
45. Frisch, M.; Trucks, G.; Schlegel, H.; Scuseria, G.; Robb, M.; Cheeseman, J.; Scalmani, G.; Barone, V.; Mennucci, B.; Petersson, G. *Gaussian 09 (Revision D.01)*; Gaussian, Inc.: Wallingford, CT, USA, 2013.
46. Macrae, C.F.; Edgington, P.R.; McCabe, P.; Pidcock, E.; Shields, G.P.; Taylor, R.; Towler, M.; van de Streek, J. Mercury: Visualization and analysis of crystal structures. *J. Appl. Crystallogr.* **2006**, *39*, 453–457. [CrossRef]
47. Bao, L.P.; Wang, B.Z.; Yu, P.Y.; Huang, C.; Pan, C.W.; Fang, H.Y.; Akasaka, T.; Guldi, D.M.; Lu, X. Intermolecular packing and charge transfer in metallofullerene/porphyrin cocrystals. *Chem. Commun.* **2019**, *55*, 6018–6021. [CrossRef]
48. Zhang, Y.; Guan, Y.N.; Chen, M.Q.; Shen, Y.P.; Pan, Q.J.; Lian, Y.F.; Yang, S.F. Favorite orientation of the carbon cage and a unique two-dimensional-layered packing model in the cocrystals of Nd@C_{82} (I, II) isomers with decapyrrylcorannulene. *Inorg. Chem.* **2021**, *60*, 1462–1471. [CrossRef] [PubMed]